ACS APPLIED MATERIALS & INTERFACES

Research Article

www.acsami.org

Noninvasive Cell-Based Impedance Spectroscopy for Real-Time Probing Inhibitory Effects of Graphene Derivatives

Keith B. Male, Edmond Lam, Johnny Montes, and John H.T. Luong*

Nanobiotechnology Group, National Research Council Canada, 6100 Royalmount Avenue, Montreal, Quebec, H4P 2R2 Canada.

ABSTRACT: Three water-dispersible graphene derivatives, graphene oxide (GO), sulfonated graphene oxide (SGO), and sulfonated graphene (SG), were prepared and probed for their plausible cytotoxicity by non-invasive electric cell-substrate impedance sensing (ECIS). With *Spodoptera frugiperda* Sf9 insect cells adhered on gold microelectrodes as an active interface, it is feasible to monitor changes in impedance upon exposure to different graphene derivatives. Sf9 insect cells were then exposed to different concentrations of graphene derivatives and their spreading and viability were monitored and quantified by ECIS in real-time. On the basis of the 50% inhibition concentration ($ECIS_{50}$), none of the graphene derivatives were judged to have any significant cytotoxicity with respect to the chosen cell line as the $ECIS_{50}$ values were all above 100 μg/mL. However, all graphene derivatives exhibited inhibitory effects on the Sf9 response at the cell spreading level with the following order: SG ($ECIS_{50}$ = 121 ± 8 μg/mL), SGO ($ECIS_{50}$ = 151 ± 9 μg/mL), and GO ($ECIS_{50}$ = 232 ± 27 μg/mL), reflecting differences observed in their ζ-potential and surface area. The presence of phenyl sulfonyl groups in SGO and SG improves their aqueous dispersity which enables these materials to have a greater inhibitory effect on Sf9 insect cells in comparison to GO. Such results were corroborated well with the cell count and viability by the Trypan Blue exclusion assay.

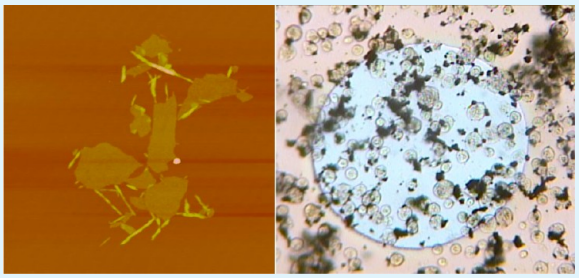

KEYWORDS: *graphene, cytotoxicity, electric cell-substrate impedance sensing, insect cells, viability assay*

INTRODUCTION

The recent and unexpected discovery of free-standing graphene[1,2] has led to the consideration of graphene and its derivatives for numerous applications.[3−8] Graphene and its derivatives with remarkable properties are capable of quenching electron donors and protecting biomolecules from enzymatic cleavage, as well as transportation capability in living cells. Therefore, various graphene-based nanomaterials have been conjugated with biomolecules for a plethora of biomedical applications. PEGylated nano-graphene oxide (NGO, sheets a few nanometers in lateral width) is photoluminescent and could be used for live cell imaging in the near-infrared.[5] The biocompatible PEGylated NGO functionalized with antibody could also be loaded with the cancer drug doxorubicin for selective cancer cell killing in vitro. The concept has been tested successfully with tumor-bearing mice by intravenous administration and the performance compared well with methods using PEGylated gold nanorods with the added advantage of high loading capacity due to the ultrahigh surface area of the nano graphene.[6] Similar to carbon nanotubes (CNTs), graphene-based materials likely involve a three-step antimicrobial action, involving cell deposition, membrane stress due to contact with sharp nanosheets, followed by superoxide anion-dependent oxidation.[7] GO and reduced GO (RGO) were shown to inhibit growth of *E. coli* while showing insignificant cytotoxicity, thus leading to their incorporating into antibacterial paper.[8] SG acts as a water-stable catalyst for the hydrolysis of ethyl acetate,[9] whereas SGO is capable of dehydrating xylose to furfural in water.[10] Graphene has proven as a promising biocompatible scaffold that does not hamper the proliferation of human mesenchymal stem cells, but accelerates their specific differentiation into bone cells.[11]

The safety issue with regard to potential toxic/cytotoxic responses is of utmost importance for large scale production and applications of such nanomaterials. For instance, CNTs have been considered for many applications; however issues have arisen due to their possible toxic effect.[12] Conflicting results claiming both toxic and non-toxic effects of these materials have led to much controversy.[13] The difficulty in properly purifying CNTs often results in toxicity related to the starting materials (heavy metal catalysts) and byproducts rather than the CNTs themselves.[14] Similarly, graphene and its derivatives are being considered for numerous applications including nanomedicine, cancer therapy, catalysis and pollutant management.[15] The increased water solubility of sulfonated graphene materials may have more considerable consequences than non-sulfonated derivatives when disposed into the environment after usage.

A number of reports exploring the potential cytotoxic effects of graphene materials have indicated both toxic and non-toxic effects, dependent upon the cell line and the viability assay procedure.[4,16−18] In general, graphene and its derivatives

Received: April 26, 2012
Accepted: July 2, 2012
Published: July 2, 2012

exhibit biocompatibility with human cells[19] and graphene per se is a good candidate for the adhesion and proliferation of L929 cells.[20] Human osteoblasts and mesenchymal stromal cells adhere and proliferate better when cultured on the chemical vapor deposition (CVD) grown graphene than on a SiO_2 substrate.[21] The CVD-grown graphene film serves as a substrate of neuritis and significantly enhances the cell growth during 2-7 days after cell seeding compared with tissue culture polystyrene substrates.[22] A Tween/reduced graphene oxide (RGO) hybrid paper was shown to have no cytotoxic effects when tested with three different mammalian cell lines.[23] For biomedical applications such as drug delivery, cancer therapy, cell imaging, etc., it is straightforward to activate epoxide and ester groups of graphene derivatives and convert hydroxyl groups to carboxylic acid moieties for subsequent bioconjugation.[24]

Electric cell-substrate impedance sensing (ECIS) is capable of probing cytotoxicity of toxicants without the above mentioned interferences.[25] Upon inoculation, cells settle on the bottom of tissue culture wells, each containing a microfabricated circular gold electrode, precoated with a binding protein, known as the extracellular matrix. Eventually, the confluent cell layer formed affects the current flow, as these adhered cells will act as insulating particles because of their plasma membrane. Impedance change, reflecting toxicity effect, can be monitored and quantified[26] when cells are exposed to noxious agents,[27] heavy metals and nitrotoluenes,[28,29] nanomaterials,[30] and drugs.[31]

Although ECIS has been conducted extensively for probing cytotoxicity of chemicals, drugs, etc., its demonstration for nanoscale materials is very limited and to the best of our knowledge, this technique has not been proven for graphene and its sulfonated derivatives. Nearly all materials exhibit toxicity at a high enough concentration. Therefore, robust, rapid, and cost effective analytical techniques will be required to assess any plausible toxicity of such engineered nanomaterials in air, water, and soil. It has come to attention that *Sf*9, a lepidopteran cell line isolated from the fall armyworm, *Spodoptera frugiperda*, is significantly more resistant to growth inhibition induced by chemicals such as hydrogen peroxide, bleomycin, streptonigrin, etc. and apoptosis induction effects of X-ray irradiation than several human cell lines of different origins.[32]

This paper reveals the applicability of ECIS together with the insect cell for probing cytoxicity of graphene derivatives in real time. The approach is based on correlating the behavior of insect cells at interface with an electronic platform used as a proxy, with the complex internal cellular signaling induced by exposure to graphene derivatives. Using the cells immobilized on gold microelectrodes as an active interface, it is feasible to monitor changes in impedance upon exposure to different graphene derivatives. ECIS together with the insect cell serves as a litmus test for non-invasive probing cytotoxicity of nanoscale materials and their metabolites in real time using a high throughput electronic platform.

The ECIS method provides multiple chambers for continuous parallel or replicate measurements on small numbers of cells. This approach provides a better temporal resolution for toxicity profiles because the standard end point measurement performed by the standard fluorescence labeling, FCA and MTT assays may neglect the intermediate time events. Of course, such experiments could have been performed at additional time points, but at the cost of significantly increased effort and experimental replication.

EXPERIMENTAL METHODS

Materials. Concanavalin A, graphite powder, sulfuric acid, hydrochloric acid, potassium persulfate, phosphorus pentaoxide, potassium permanganate, hydrogen peroxide (30%), hydrazine, sodium borohydride, sodium carbonate, sulfanilic acid, and sodium nitrite were obtained from Sigma-Aldrich and used as received.

Synthesis of Graphene Derivatives. Graphene derivatives were prepared as previously described.[10] GO was synthesized using the modified Hummers' method.[33,34] In brief, 10 g of pre-oxidized graphite (reacted with H_2SO_4, $K_2S_2O_8$, and P_2O_5) was added to ice-cold H_2SO_4, followed by the slow addition of $KMnO_4$ at 35 °C for 2 h. The acidic graphite solution was then slowly poured into a solution of 30% H_2O_2 in water. The resultant brown solution was washed with 10% HCl solution and centrifuged three times at 10 000 rpm for 20 min. The resulting brown residue was dialyzed and freeze-dried as GO.

SGO and SG were prepared by the Samulski method.[35] In brief, dissolved $NaBH_4$ was added dropwise to GO, which had been dispersed in water by sonication. The pH was adjusted to 9.1 by the addition of Na_2CO_3 solution and the mixture was heated at 80 °C for 1 h. The resulting black mixture was washed and centrifuged as described above. The partially reduced GO was redispersed in water by sonication and cooled. A diazonium salt solution (prepared from an aqueous solution of sulfanilic acid, HCl, and $NaNO_2$) was poured into the ice-cold GO solution and stirred overnight. After washing and centrifugation, the resulting black residue was dialyzed and freeze-dried as SGO. To prepare SG, SGO was dispersed in water by sonication followed by the addition of hydrazine. The suspension was heated for 24 h at 100 °C with constant stirring. The black suspension was washed and centrifuged as described above. The resultant black residue was dialyzed and freeze-dried as SG.

Characterization of Graphene Derivatives. The structure and chemical composition of the graphene derivatives were confirmed by scanning electron microscopy-energy dispersive X-ray (SEM-EDX) (Hitachi S 2600N SEM, Hitachi Scientific Instruments, Tokyo, Japan) equipped with a microanalysis detector for EDX (Inca x-act, Oxford Analytical Instruments, Abington, UK), low voltage transmission electron microscopy (LVTEM) (Delong LVEM, Soquelec, Montreal, QC, Canada), fourier transform infrared (FTIR) spectroscopy (Bruker Tensor 27 FTIR spectrophotometer), Raman spectroscopy (LabRAM HR 800, Horiba/Jobin-Yvon, Longjumeau, France) equipped with an Ar-ion 514.5 nm laser operating at 200 mW, as described previously.[10] Further structural characterization was performed using atomic force microscopy (AFM) (Dimension 3100 with a NanoScope IV controller, Veeco Digital Instruments, Santa Barbara, CA) using tapping mode with a silicon cantilever (MPP-11100, spring constant ~40 N/m, resonance frequency ~300 kHz, NanoDevices, CA) at scan rates of 0.5 Hz with 512×512 pixels. ζ-potential of graphene derivatives (400 μg/mL) in water and SF-900 II medium (Gibco BRL, Canadian Life Technologies, Burlington, ON, Canada) were determined using a Zetasizer Nano-ZS (Malvern Instruments, Malvern, UK) in triplicate.

Cell Line and Culture Conditions. *Spodoptera frugiperda Sf*9 cells were maintained in 125 mL-disposable Erlenmeyer flasks with a working volume of 20 mL in serum-free SF-900 II medium. Cells were cultured weekly at 0.4×10^6 cells/mL at 27 °C, pH 6.2, with agitation at 110 rpm. During the growth, the cell count and viability by the Trypan Blue exclusion assay were performed with a CEDEX Innovatis cell counter (Bielefeld, Germany). *Sf*9 cells, inoculated at an initial cell density of 0.4×10^6 cells/mL, were grown to the mid-exponential phase $2.5\text{-}3 \times 10^6$ cells/mL and the resulting cells were aseptically centrifuged at 1500 rpm for 4 min. Pellets were thereafter suspended at a cell concentration of 3×10^6 cells/mL in a fresh medium.

Electrode Coating and Cell Addition. Concanavalin A (Con A, 0.40 mL, 0.5 mg/mL, prepared fresh daily in 50 mM PBS, pH 7.4 with sonication for 1 h) was added into each of the 8 wells of a sensing chip (8W1E, Applied Biophysics, Troy, NY) to coat the detecting gold electrodes as previously described.[28] Con A binds quickly (90% of the

change occurs in the first 10 min) to the electrode surface as confirmed by an impedance increase. After protein adsorption (~30-60 min), the wells were washed 3 times with 0.85% NaCl and 0.4 mL of culture medium was placed in each well. The impedance baseline was monitored for 1-2 h at 27 °C in a humidified chamber with the ECIS impedance system and then the wells were emptied before the addition of the cell-graphene derivative suspension. Graphene derivative samples (~10 mg/mL) were sonicated for 20 min (Branson Ultrasonics Corp, Danbury, CT) before addition (5-60 μL) to the *Sf*9 insect cell suspension (1.5 mL at 3 × 10^6 cells/mL containing 2% EtOH) resulting in various concentrations (35-400 μg/mL). For testing possible inhibitory effects, 0.4 mL of each sample concentration was added to 2 wells. For each graphene derivative sample, 6 concentrations including a control (no graphene derivatives) were tested at the same time and each derivative was analyzed at least 3 different times.

Impedance Measurement. The ECIS system measures up to 16 sample wells (2 chips of 8 wells, each containing a singly addressable detecting electrode) per experiment.[28] A common counter gold electrode is shared by the 8 detecting electrodes and the two electrodes (detecting gold electrode and counter gold electrode) of the well are connected to a lock-in amplifier. The well impedance was measured every 2 min at 1 VAc and 4 kHz, and the system acquires resistance, impedance and capacitance data. The oscillator applies an AC signal of amplitude 1 V through a series 1 MΩ resistor to the two-electrode system. With this setup and using culture medium as the electrolyte, the current flow is constant at ~1 mA. At this operating condition, the current exhibits no effect on cell behavior and proliferation. As larger changes occurred in the resistance we have focused on these changes in this study. The $ECIS_{50}$ value derived from the time response function, $f(C,t)$, was calculated as previously described.[29] For simplification of plots and calculations, data points at 30 min intervals were selected from the raw resistance data. After the experiment, cells were imaged using a Wilovert AFL 30 inverted microscope (Hund, Germany) equipped with a digital video camera (KP-D50U, Hitachi, Tokyo, Japan).

RESULTS AND DISCUSSION

Characterization of Graphene Derivatives. As previously reported, SEM images of the three graphene derivatives adopt a crumpled, layered structure with sheetlike appearances in their LVTEM images (not shown).[10] AFM images of the three graphene derivatives dried on a mica surface show that the nanosheets have a thickness of about 1 nm (Figure 1).

In Raman spectroscopy, blue shifts were observed for the G band in GO, SGO, and SG compared to graphene (1348 cm^{-1}) which is consistent with chemical doping of the graphene sheet.[36] Although an exact structure of GO remains to be deciphered, carboxylic acid groups are only present in very low quantities at the periphery of the graphitic platelets, in addition to other keto groups.[37−39] In this study, the spectrum of GO shows peaks at 1728 cm^{-1} ($\nu_{C=O}$), 1384 cm^{-1} (ν_{C-OH}), 1273 cm^{-1} (ν_{C-O-C}), and 1061 cm^{-1} (ν_{C-O}), for the carbonyl, hydroxyl, and epoxide groups, respectively. FTIR spectroscopy peaks at 1165 cm^{-1} (ν_{S-O}), 1124 cm^{-1} (ν_{S-O}), and 1033 cm^{-1} ($\nu_{S\text{-Phenyl}}$) confirmed the presence of phenyl sulfonic acid groups on SGO and SG.[10] With SGO and SG, peaks for the carbonyl groups were diminished, leading to a reduction in oxygen content, confirmed by EDX analysis.[10]

Response of *Sf*9 Insect Cells. The gold microelectrode was fully covered by Con A; a lectin purified from *Concanavalis ensiformis*. The culture medium resistance without cells was ~2.3 kΩ while with cells there was a slight increase to ~2.8 kΩ. Without the graphene samples, the cells descended to the well bottom within 20 min and changed their morphology from round to flattened forms with much larger dimensions as

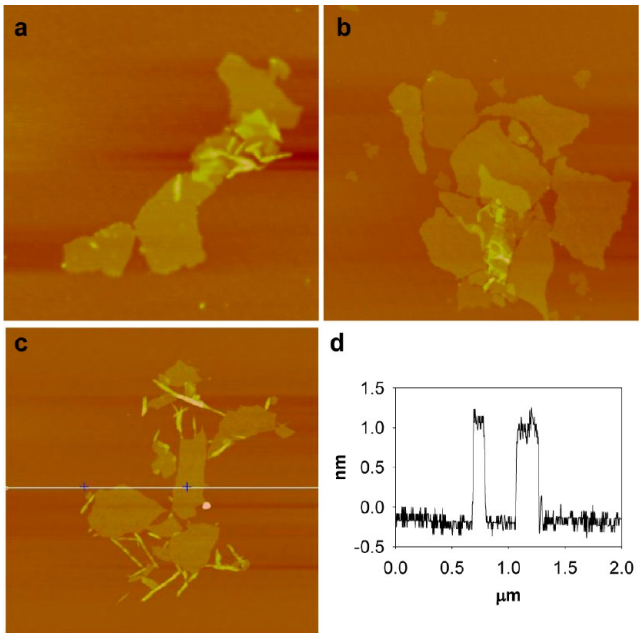

Figure 1. AFM images (a) GO, (b) SGO, and (c) SG with the corresponding height profile (d).

observed by the video-enhanced microscope. Upon cell spreading, the effective area available for current flow altered significantly, resulting in a final resistance of 9.0 kΩ or a change of ~6.2 kΩ (Figure 2A, curve a). Considering the number of normal *Sf*9 cells (150−200 cells) to completely cover an 8W1E detecting electrode coated with Con A,[28] the estimated resistance change contributed by each attached cell was 30−40 Ω/cell.

Low concentrations of graphene derivatives (≤67 μg/mL) exhibited only a modest effect on the resistance signal (Figure 2A, curve b). However, as the concentration was increased (133-400 μg/mL), the resistance change decreased significantly (Figure 2A, curves c−g). It is important to note that the graphene derivatives had no effect on the resistance response in the absence of insect cells.

Half-Inhibition Concentration ($ECIS_{50}$) for GO. The resistance change (ΔR_s) of the well is dependent on the number (N_o) of initial cells attached on the detecting electrode, the toxicant concentration (C) and the exposure time (t).[29] The resistance change normalized by N_o is defined as the cell response to the toxicant measured by ECIS, $f(C,t) = \Delta R_s/N_o$. As a control with no toxicant, C is equal to zero and $f(0,t)$ increases as the cells spread on the electrode and reaches a plateau. In the presence of the toxicant, $f(C,t)$ increases initially, and then the value decreases and can even approach zero, indicating total cell death at high toxicant concentrations. The inhibitor concentration required to achieve 50% inhibition of the response is defined as the half-inhibition concentration ($ECIS_{50}$) or $f(ECIS_{50},t)/f(0,t) = 50\%$.

The $ECIS_{50}$ for GO was calculated from the data obtained in Figure 2A. The time response function $f(C, t)$ was used to construct a series of inhibition curves at any given time t_0 (≥ 2.5 h) for the different GO concentrations used in Figure 2A. The presence of GO did not interfere with the initial settling of the insect cells; although the spreading was not as evident as time progressed, especially at high concentrations of GO. N_o for each well was assumed to be equivalent, therefore no adjustment for ΔR_s was required due to different N_o values.

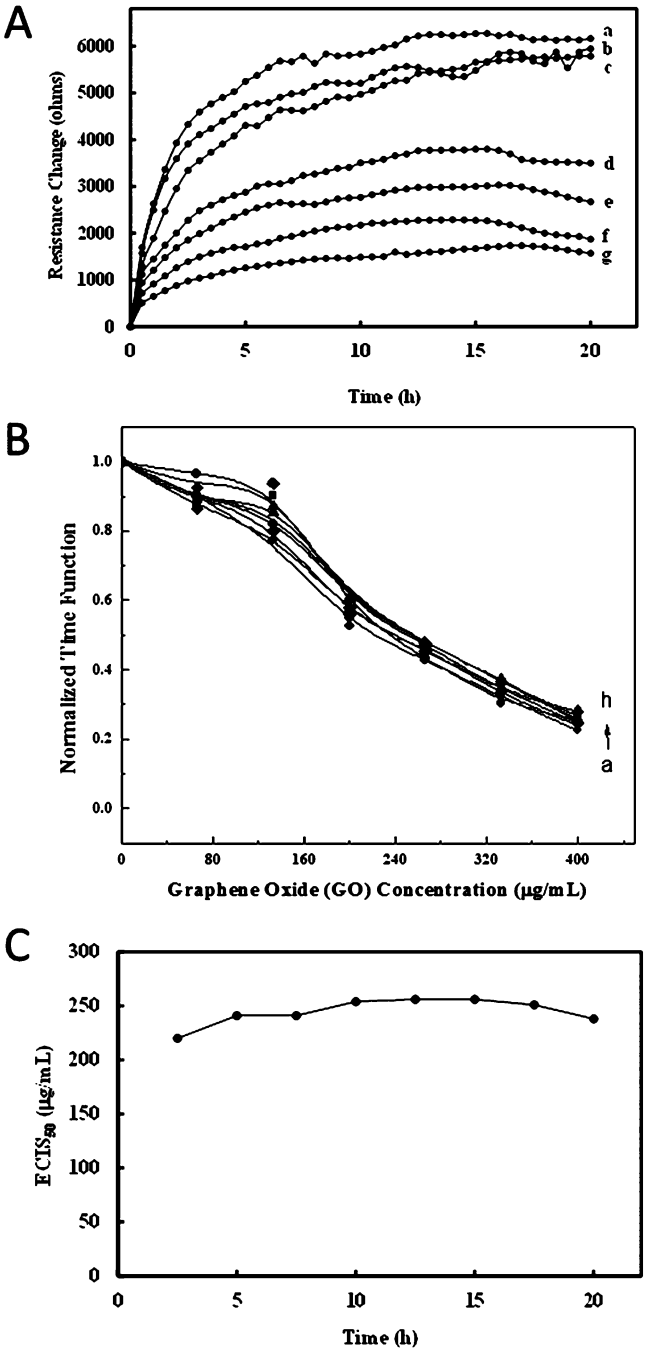

Figure 2. (A) Resistance response (Ω) of *Sf*9 insect cells to various concentrations (μg/mL) of GO: (a) 0, (b) 67, (c) 133, (d) 200, (e) 267 (f) 333, and (g) 400. (B) GO inhibition curves were obtained for each GO concentration (Figure 2A, curves a-g) at various exposure times (h): (a) 2.5, (b) 5.0, (c) 7.5, (d) 10, (e) 12.5, (f) 15, (g) 17.5, and (h) 20. The normalized time response function (*Y* axis), $f(C,t)$, was determined by taking the ΔR_s (A, curves b−g), i.e., $R_t - R_0$ at different NCC concentrations and dividing the values by the ΔR_s (~6200 Ω, A, curve a) at $f(0, t)$. (C) Relationship between the half-inhibition concentration ($ECIS_{50}$) and exposure time during cell culture for GO. The $ECIS_{50}$ value obtained for GO was determined for each exposure time (B, curves a−h) by extrapolating the value for the *X*-axis from the *Y*-axis (0.5).

The time response function, $f(C,t)$, was then normalized by simply taking the ΔR_s, i.e., R_t-R_0 at different GO concentrations and dividing these values by the ΔR_s value at $f(0, t)$. The normalized time response function decreased as expected as the concentration of GO increased for all exposure times (Figure 2B).

The $ECIS_{50}$ for GO was determined for each exposure time by extrapolating the value on the GO concentration axis when the normalized time response function was 0.5. Figure 2C shows the relationship between the half-inhibition concentration and exposure time, indicating that the $ECIS_{50}$ for GO was similar (245 ± 10 μg/mL, 95% confidence interval) over a wide range of exposure times (2.5−20 h). The result indicated that there was no lag time before the GO displayed the inhibitory effect. Owing to the rapid settling of the cells on the surface at high cell concentration, the $ECIS_{50}$ value was a reflection of the interference or inhibition capacity of GO with respect to the cell spreading on the substratum. Hence, the effect of the GO on the ECIS response was not significantly cytotoxic, but likely inhibitory at the level of cell adherence and spreading on the substratum layer.

Inhibitory Effect of Other Graphene Derivatives. ECIS experiments were also conducted using SGO and SG. The inhibition effect of these two derivatives was stronger when compared to the $ECIS_{50}$ value of 232 ± 27 μg/mL (95% confidence interval) observed for GO (Figure 3). Exposure to

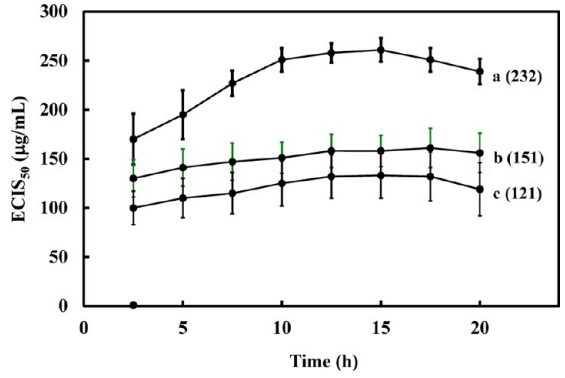

Figure 3. Relationship between the half-inhibition concentration and time, during cell culture for different graphene derivatives with data expressed as SEM, n = 4−6, $ECIS_{50}$ value in brackets: (a) GO, (b) SGO, and (c) SG.

SGO resulted in an $ECIS_{50}$ value of 151 ± 9 μg/mL (95% confidence interval), whereas SG had the lowest $ECIS_{50}$ value of 121 ± 8 μg/mL (95% confidence interval). The results could possibly be correlated to the solubility and dispersion of the graphene derivatives.

Inverted fluorescent microscopy (Figure 4A) confirmed that the insect cells in the absence of graphene derivatives were intact and well spread on the Con A coated electrode surface even after washing the wells with PBS 3 times. However, cells exposed to SG (300 μg/mL) for 24 h were more spherical and not as well spread on the electrode surface resulting in numerous gaps (Figure 4B) when compared to the control cells. SG particles in the form of aggregates were noted on the surface of the cells and similar images were observed with GO and SGO. Such results were in agreement with the work that showed that GO does not enter A549 cell and exhibits no obvious cytotoxicity.[40] Strong cytotoxic effects with the ECIS system normally result in cells delaminating from the surface and the resistance change would return to zero. However, graphene derivatives still cause a dose-dependent oxidative

dx.doi.org/10.1021/am301060z | ACS Appl. Mater. Interfaces 2012, 4, 3643−3649

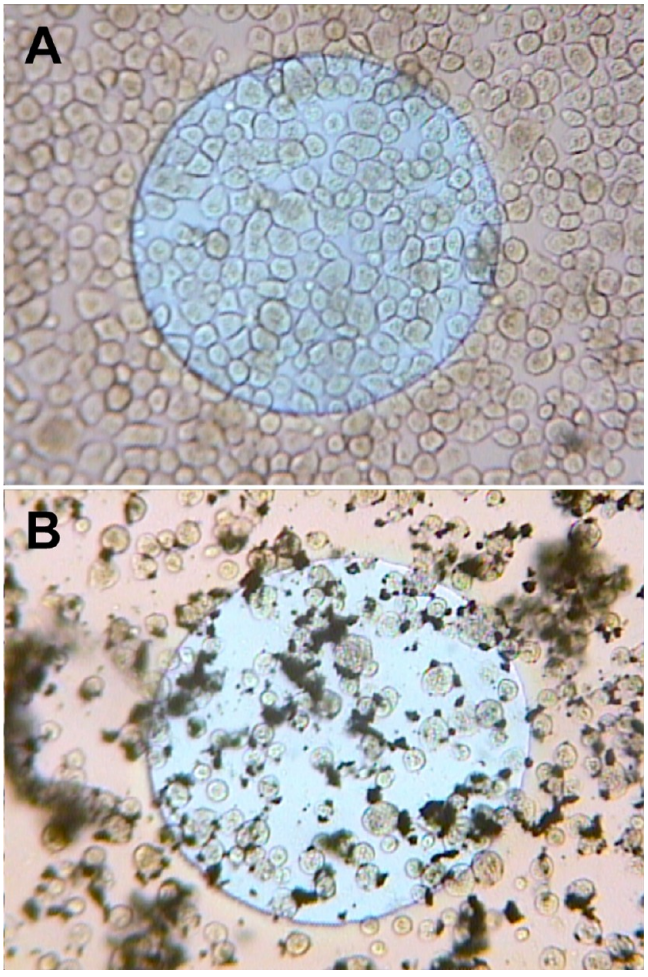

Figure 4. Microscopic photos of the electrode surface after 24 h: (A) without SG and (B) with 300 μg/mL SG. Note: The blue circle is the gold electrode surface having a diameter of 250 μm.

stress in the cell, resulting in a slight loss of cell viability at high concentration.

Surface charge and colloidal stability of graphene derivatives in water and SF-900 II medium (at 400 μg/mL) were obtained by ζ-potential measurements and visual evidence of settling. It should be noted that the ζ-potential can be related to the stability of colloid dispersion and a high zeta potential (negative or positive above 40 mV) will confer stability.[41] All ζ-potentials were negative in value (Table 1). For aqueous solutions, SGO and SG both had lower ζ-potentials (−36.2 and −31.9 mV) than GO (−21.5 mV), indicating moderate stability for SGO and SG and incipient instability for GO. The colloidal stability of the SGO and SG solutions was evident from aqueous solutions left to stand for 24 h in comparison to the GO solution (Figure 5A−C). Aggregation of graphene derivatives in SF-900 II medium was faster (Figure 5D−F) with ζ-potentials much less negative than those obtained in water. The accelerated aggregation of graphene derivatives could be attributed to the screening of electrostatic charges in solutions rich in salts.[42] Furthermore, all graphene derivatives solutions (400 μg/mL) prepared by 20 min bath sonication aggregated within 2 h and exhibited higher ζ-potential values (GO, −4.60 ± 0.19 mV; SGO, −5.87 ± 0.95 mV; SG, −5.39 ± 0.22 mV) than their probe-sonicated counterparts.

Table 1. ζ-Potential Values (Mean ± Standard Deviation) for Graphene Derivative Solutions (400 μg/mL) Prepared by Probe Sonication for 30 s

sample	ζ-potential in water (mV)	ζ-pPotential in SF-900 II medium (mV)
GO	−21.5 ± 0.8	−6.25 ± 0.50
SGO	−36.2 ± 0.7	−9.38 ± 0.98
SG	−31.9 ± 0.7	−6.98 ± 0.39

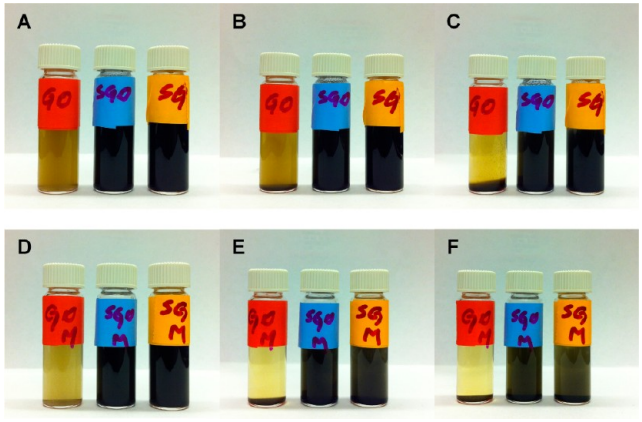

Figure 5. Photos of free-standing solutions of graphene derivatives in water at (A) 0, (B) 6, and (C) 24 h and in SF-900 II medium at (D) 0, (E) 6, and (F) 24 h. The 400 μg/mL graphene solutions were prepared by probe sonication for 30 s (1000 J).

Similar patterns of solubility and dispersion have been reported previously for four graphene related materials. In brief, GO with carboxyl, hydroxyl and epoxy groups should result in more stable dispersions compared to ones with hydrophobic pristine carbon chains (graphite and RGO), resulting in better opportunities for cell interaction and antibacterial activity.[7] Due to the addition of sulfonyl groups SGO and SG are even more stable in solution than GO. It should be noted that the surface area of GO (318 m^2/g) is about half of SGO (680 m^2/g) and SG (634 m^2/g),[10] and that the $ECIS_{50}$ value for GO is about double the value for the other derivatives. The cytotoxic activity of amorphous silica nanoparticles (SNPs) has been link to surface area rather than aggregation with SNPs of low specific surface area responsible for lower cytotoxic effects.[43]

The Trypan Blue exclusion assay confirmed that graphene derivatives were not significantly cytotoxic to the insect cells in the concentration range used during the experiment although inhibition of growth was observed. Cell counting performed at 0, 3, 6, and 24 h indicated that cell viability was still above 84% when cells were exposed to 50 or 200 μg/mL of GO, SGO, or SG, corresponding well with the ECIS data whereby most of the cells still remained intact on the electrode surface. Cell viability of the control sample was constant at 99% throughout the experiment. Cell viability for GO dropped to 96 and 94% after 24 h at 50 and 200 μg/mL, respectively. Results for SGO after 24 h were similar with values of 97 and 91% viability for 50 and 200 μg/mL, respectively. Exposure to SG resulted in the most significant drop in viability with values of 93 and 84% for 50 and 200 μg/mL, respectively. The viability values at 3 h were very similar to those at 24 h indicating that there was an initial drop in viability which then remained relatively constant with time. There was a noticeable effect of GO, SGO, and SG (50 or 200 μg/mL) on the cell growth over the experimental course as the cell densities were different from the control. The viable cell

density of the control increased from 2.6×10^6 cells/mL to 4.4×10^6 cells/mL over the 24 h period. In comparison, after 24 h the viable cell densities were 3.4×10^6, 3.8×10^6, and 2.9×10^6 cells/mL for GO, SGO, and SG (50 μg/mL), respectively. These results were corroborated well with the ECIS results indicating the most inhibitory effect of SG on the cells.

Half-Inhibition Concentration Obtained by $ECIS_{50}$ vs Literature Data. The half-inhibition concentration obtained by $ECIS_{50}$ for three graphene derivatives deserves some comments here. Table 2 is a brief survey of the influence of various graphene derivatives on different cell lines towards cytoxicity.

Table 2. Survey of Cytotoxic Effects of Different Cell Lines with Various Graphene Derivatives

sample	effect	reference
GO	50 μg/mL can induce cytotoxicity in human fibroblast cells	17
GO	85 μg/mL decreases A549 cell proliferation	18
RGO	85 μg/mL induces strong antibacterial activity on *E. coli* DH5α cells	8
RGO/Tween hybrid	no cytotoxicity on Vero (African green monkey kidney cells), Embryonic bovine and Crandell-Rees feline kidney cells	23
PEGylated GO	no cytoxicity on Raji and HCT-116 up to 100 mg/L	5, 42
Fluorescent GO	no cytoxicity on Hep G2 at 400 mg/L (MTT assay)	44
GO/TiO_2 hybrid	no cytoxicity with HeLa cells up to 100 mg/L during long incubation time	45

Toxicity testing of carbon nanotubes with the conventional MTT viability assay has led to problems in interpretation due to the binding and interference of the nanomaterial with the dye.[46] A549 human alveolar epithelial cells incubated with single-walled carbon nanotubes (SWCNTs) faked a strong cytotoxic effect of 50% after 24 h with the MTT assay, whereas other detection methods such as the release of lactate dehydrogenase (LDH) after membrane damage revealed no cytotoxicity. Indeed, graphene and GO have been shown to give a false positive result associated with the MTT assay.[47]

CONCLUSIONS

In brief, an on-line and continuous technique based on electric cell-substrate impedance sensing (ECIS) has been applied for measuring the concentration and time response function of *Sf*9 insect cells exposed to three water-dispersible graphene derivatives. The presence of phenyl sulfonyl groups in SGO and SG allows for the formation of stable colloids which enables these materials to have a greater inhibitory effect on *Sf*9 insect cells in comparison to GO. Non-cytotoxicity of graphene derivatives warrants the development of this renewable material for biomedical applications. As large scale productions of graphene and its derivatives are being constantly improved, these nanoscale materials with the highest Young's modulus (0.5−1 TPa) might find important and successful applications in implants, the repair of injured tissues and other stem cell-based regenerative medicine strategies. Further studies to understand the cytotoxicity of graphene derivatives with human cell lines will be required to assess biocompatibility. Cell-based impedance spectroscopy measurement in combination with *Sf*9 cells or other cell lines is a simple and reliable tool for screening potentially cytotoxic/inhibitory effects of nanoscale materials. This noninvasive and real-time approach allows quantitative assessment of biocompatibility of lead nanoscale materials for diversified biomedical applications.

AUTHOR INFORMATION

Corresponding Author

*E-mail: john.luong@cnrc-nrc.ga.ca. Telephone: +1 514 496 6175. Fax: +1 514 496 6265.

Notes

The authors declare no competing financial interest.

ACKNOWLEDGMENTS

The authors thank Yali Liu of the National Research Council Canada (NRC), Montreal, Quebec, Canada, for performing atomic force microscopy (AFM).

REFERENCES

(1) Novoselov, K. S.; Geim, A. K.; Morozov, S.V.; Jiang, D.; Zhang, Y.; Dubonos, S. V.; Grigorieva, I. V.; Firsov, A. A. *Science* **2004**, *306*, 666−669.
(2) Novoselov, K. S.; Jiang, D.; Schedin, F.; Booth, T. J.; Khotkevich, V. V.; Morozov, S. V.; Geim, A. K. *Proc. Natl. Acad. Sci. U.S.A.* **2005**, *102*, 10451−10453.
(3) Geim, A.K.; Novoselov, K.S. *Nat. Mater.* **2007**, *6*, 183−191.
(4) Li, X.; Wang, X.; Zhang, L.; Lee, S.; Dai, H. *Science* **2008**, *319*, 1229−1230.
(5) Sun, X. M.; Liu, Z.; Welsher, K.; Robinson, J. T.; Goodwin, A.; Zaric, S.; Dai, H. J. *Nano Res.* **2008**, *1*, 203−212.
(6) Yang, K.; Zhang, S.; Zhang, G.; Sun, X.; Lee, S. -T.; Liu, Z. *Nano Lett.* **2010**, *10*, 3318−3323.
(7) Liu, S.; Zeng, T. H.; Hoffmann, M.; Burcombe, E.; Wei, J.; Jiang, R.; Kong, J.; Chen, Y. *ACS Nano* **2011**, *5*, 6971−6980.
(8) Hu, W.; Peng, C.; Luo, W.; Lv, M.; Li, X.; Li, D.; Huang, Q.; Fan, C. *ACS Nano* **2010**, *4*, 4317−4323.
(9) Ji, J.; Zhang, G.; Chen, H.; Wang, S.; Zhang, G.; Zhan, F.; Fan, X. *Chem. Sci.* **2011**, *2*, 484−487.
(10) Lam, E.; Chong, J. H.; Majid, E.; Liu, Y.; Hrapovic, S.; Leung, A. C. W.; Luong, J. H. T. *Carbon* **2012**, *50*, 1033−1043.
(11) Nayak, T. R.; Andersen, H.; Makam, V. S.; Khaw, C.; Bae, S.; Xu, X.; Ee, P. -L. R.; Ahn, J. -H.; Hong, B. H.; Pastorin, G.; Özyilmaz, B. *ACS Nano* **2011**, *5*, 4670−4678.
(12) Son, S. J.; Reichel, J.; He, B.; Schuchman, M.; Lee, S. B. *J. Am. Chem. Soc.* **2005**, *127*, 7316−7317.
(13) Hussain, M.A.; Kabir, M.A.; Sood, A.K. *Curr. Sci.* **2009**, *96*, 664−673.
(14) Colvin, V. *Nat. Biotechnol.* **2003**, *21*, 1166−1170.
(15) Zhao, G.; Jiang, L.; He, Y.; Li, J.; Dong, H.; Wang, X.; Hu, W. *Adv. Mater.* **2011**, *23*, 3959−3963.
(16) Zhang, Y. B.; Ali, S. F.; Dervishi, E.; Xu, Y.; Li, Z.; Casciano, D.; Biris, A. S. *ACS Nano* **2010**, *4*, 3181−3186.
(17) Wang, K.; Ruan, J.; Song, H.; Zhang, J.; Wo, Y.; Guo, S.; Cui, D. *Nanoscale. Res. Lett.* **2011**, *6*, 8.
(18) Ryoo, S. R.; Kim, Y. K.; Kim, M. H.; Min, D. H. *ACS Nano* **2010**, *4*, 6587−6598.
(19) Tong, S.C. *eXPRESS Polym. Lett.* **2012**, *6*, 437.
(20) Chen, H.; Müller, M. B.; Gilmore, K. J.; Wallace, G. G.; Li, D. *Adv. Mater.* **2008**, *20*, 3557−3561.
(21) Kalbacova, M.; Broz, A.; Kong, J.; Kalbac, M. *Carbon* **2010**, *48*, 4323−4329.
(22) Li, N.; Zhang, X. M.; Song, Q.; Su, R.; Zhang, Q.; Kong, T.; Liu, L.; Jin, G.; Tang, M.; Cheng, G. *Biomaterials* **2011**, *32*, 9374−9382.
(23) Park, S.; Mohanty, N.; Suk, J. W.; Nagaraja, A.; An, J.; Piner, R. D.; Cai, W.; Dreyer, D. R.; Berry, V.; Ruoff, R. S. *Adv. Mater.* **2010**, *22*, 1736−1740.
(24) Hermanson, G. T. *Bioconjugate Techniques*; Academic Press: San Diego, 1996.
(25) Mitra, P.; Keese, C. R.; Giaever, I. *Biotechniques* **1991**, *11*, 504−511.

(26) Kowolenko, M.; Keese, C. R.; Lawrence, D.A.; Giaever, I. *J. Immunol. Methods* **1990**, *127*, 71−77.
(27) Lo, C.-M.; Keese, C.R.; Giaever, I. *Exp. Cell Res.* **1993**, *204*, 102−109.
(28) Luong, J. H. T.; Habibi-Razaei, M.; Meghrous, J.; Xiao, C.; Male, K. B.; Kamen, A. *Anal. Chem.* **2001**, *73*, 1844−1848.
(29) Xiao, C.; Lachance, B.; Sunahara, G.; Luong, J. H. T. *Anal. Chem.* **2002**, *74*, 5748−5753.
(30) Male, K. B.; Leung, A. C. W.; Montes, J.; Kamen, A.; Luong, J. H. T. *Nanoscale* **2012**, *4*, 1373−1379.
(31) Male, K. B.; Rao, Y. K.; Tzeng, Y.-M.; Montes, J.; Kamen, A.; Luong, J. H. T. *Chem. Res. Toxicology.* **2008**, *21*, 2127−2133.
(32) Cheng, I. -C.; Lee, H. -J.; Wang, T. C. *Mutagenesis* **2009**, *24*, 259−269.
(33) Hummers, W.S.; Offeman, R.E. *J. Am. Chem. Soc.* **1958**, *80*, 1339.
(34) Kovtyukhova, N. I.; Olivier, P. J.; Martin, B. R.; Mallouk, T. E.; Chizhik, S. A.; Buzaneva, E. V.; Gorchinskiy, A. D. *Chem. Mater.* **1999**, *11*, 771−778.
(35) Si, Y.; Samulski, E.T. *Nano Lett.* **2008**, *8*, 1679−1682.
(36) Ferrari, A. C.; Meyer, J. C.; Scardeli, V.; Casiraghi, C.; Lazzeri, M.; Mauri, F.; Piscanec, S.; Jiang, D.; Novoselov, K. S.; Roth, S.; Geim, A. K. *Phys. Rev. Lett.* **2006**, *97*, 187401.
(37) Scholz, W.; Boehm, H. P. *Z. Anorg. Allg. Chem.* **1969**, *369*, 327−340.
(38) Hadzi, D.; Novak, A. *Faraday Trans.* **1955**, *51*, 1514.
(39) Rodriguez, A. M.; Jimenez, P. S. V. *Carbon* **1986**, *24*, 163−167.
(40) Chang, Y.; Yang, S. -T.; Liu, J. -H.; Dong, E.; Wang, Y.; Cao, A.; Liu, Y.; Wang, H. *Toxicol. Lett.* **2011**, *200*, 201−210.
(41) Hunter, R.J. *Foundations of Colloid Science*; Oxford University Press, Oxford, 1989.
(42) Liu, Z.; Robinson, J. T.; Sun, X. M.; Dai, H. J. *J. Am. Chem. Soc.* **2008**, *130*, 10876−10877.
(43) Rabolli, V.; Thomassen, L. C. J.; Uwambayinema, F.; Martens, J. A.; Lison, D. *Toxicol. Lett.* **2011**, *206*, 197−203.
(44) Xie, G.; Cheng, J.; Li, Y.; Xi, P.; Chen, F.; Liu, H.; Hou, F.; Shi, Y.; Huang, L.; Xu, Z.; Bai, D.; Zeng, Z. *J. Mater. Chem.* **2012**, *22*, 9308−9314.
(45) Hu, Z.; Huang, Y.; Sun, S.; Guan, W.; Yao, Y.; Tang, P. *Carbon* **2012**, *50*, 994−1004.
(46) Worle-Knirsch, J. M.; Pulskamp, K.; Krug, H. F. *Nano Lett.* **2006**, *6*, 1261−1268.
(47) Liao, K. H.; Lin, Y. S.; Macosko, C. W.; Haynes, C. L. *ACS Appl. Mater. Interfaces* **2011**, *3*, 2607−2615.